
# Silver-choline chloride modified graphene oxide: novel nano-bioelectrochemical sensor for Celecoxib detection and CCD-RSM model

Zohreh Parsaee, Nima Karachi, Seyyed Milad Abrishamifar, Mohammad Reza Rezaei Kahkha, Razieh Razavi

PII: S1350-4177(18)30431-0
DOI: https://doi.org/10.1016/j.ultsonch.2018.03.009
Reference: ULTSON 4122

To appear in: *Ultrasonics Sonochemistry*

Received Date: 11 December 2017
Revised Date: 14 March 2018
Accepted Date: 15 March 2018

Please cite this article as: Z. Parsaee, N. Karachi, S. Milad Abrishamifar, M. Reza Rezaei Kahkha, R. Razavi, Silver-choline chloride modified graphene oxide: novel nano-bioelectrochemical sensor for Celecoxib detection and CCD-RSM model, *Ultrasonics Sonochemistry* (2018), doi: https://doi.org/10.1016/j.ultsonch.2018.03.009

# Silver-choline chloride modified graphene oxide: novel nano-bioelectrochemical sensor for Celecoxib detection and CCD-RSM model

Zohreh Parsaee [a,*], Nima Karachi [b], Seyyed Milad Abrishamifar [c], Mohammad Reza Rezaei Kahkha [d], Razieh Razavi [e]

[a] Young Researchers and Elite Club, Bushehr Branch, Islamic Azad University, Bushehr, Iran.

[b] Department of Chemistry, Islamic Azad University, Marvdasht Branch, Marvdasht, Iran.

[c] Department of Chemical Engineering, New York international university of technology and management, New York, USA.

[d] Department of Environmental Health Engineering, Zabol University of Medical Sciences, Zabol, Iran

[e] Department of Chemistry, Faculty of Science, University of Jiroft, Jiroft, Iran.

Email address: zohreh_parsaee@yahoo.com

## Abstract

In this study, silver nanoparticles modified choline chloride functionalized graphene oxide (AgNPs-ChCl-GO) was synthesized using sonochemical method and utilized as a bioelectrochemical sensor for detection of celecoxibe (CEL). The characterization studies were ultimately performed in order to acheive a more complete understanding of the morphological and structural features of the AgNPs-ChCl-GO using different techniques including FT-IR, AFM, FE-SEM, EDX, and XRD. AgNPs-ChCl-GO demonstrated a significant improvement in the reduction activity of CEL due to the enhancement in the current response compared to the bare carbon paste electrode (CPE). The optimum experimental conditions, were optimized using central composite design (CCD) methodology. The differential pulse voltammetry (DPVs) showed an expanded linear dynamic ranges of $9.6 \times 10^{-9}$- $7.4 \times 10^{-7}$ M for celecoxib in Britton-Robinson buffer in pH 5.0 with. LOD (S/N = 3) and LOQ (S/N = 10) were obtained $2.51 \times 10^{-9}$ M and $6.58 \times 10^{-9}$ M respectively. AgNPs-ChCl-GO-carbon paste electrode exhibited suitable properties and high accuracy determination of celecoxib in the human plasma sample.

**Keywords**: Biosensor; silver nanoparticles; Choline chloride; Graphene oxide; Celecoxib; CCD.

## 1. Introduction

Nonsteroidal anti-inflammatory drugs (NSAIDs) are the most important prescribed anti inflammation drugs worldwide that used as inhibitor to treat pain, arthritis, rheumatism, colonic polyps, and menstrual cramps [1-3]. This category of drugs can effect on reducing the risk of developing Alzheimer's disease and delaying its onset [4, 5]. Celecoxib, 4-[5-(4-methylphenyl)-3-(trifluoromethyl)-1H-pyrazol-1-yl] benzene sulphonamide is a persistent member of NSAID group against biological degradation that retains its chemical structure long enough to do its healing work [6]. Also, due to its frequent application, it could remain in the environment for a long time, and its presence is considered lethal. Up to now, various methods were used for the removal of different pharmaceutical compounds from the wastewater including spectrophotometric [7-9], electrophoretic [10], chromatographic [11], fluorometric [12], polarographic [13], membrane [14], submerged aerated biological filter [15], photocatalytic degradation [16] and so on [17-23]. Electrochemical sensors are the most beneficial procedure due to their effectiveness, reasonable operational costs, no secondary pollutants generated, regeneration and reuse possibilities, short retention time, and high efficiency [24]. Therefore, the search for new types of electrochemical sensor and development of new efficient removal methods is mandatory [25-28]. Carbon based compounds are extensively used in drug sensing application due to having a potential for forming electrochemical platform with high surface area [29-33]. Among the Carbon based compounds, Graphene has attracted much attention because of their unique properties, including high values of its Young’s modulus, fracture strength [34], thermal conductivity [35], mobility of charge carriers [36], specific redox peaks [37] and specific surface area [38]. Its excellent physicochemical properties make it a suitable choice for applications in nanosensor technology [39, 40]. Meanwhile, the presence of different hydrophilic agents including hydroxyl, epoxy and acidic groups and strongly oxygenated functional groups [41] facilitate its dispersion in various solvents with long-term stability [42]. So, recently, electrochemical sensors based on GO have been applied for detection and removal of drugs. In spite of unique advantages of Go, it exhibited weak catalytic performance in some cases due to its poor conductivity [43], different approaches have been used by modifying the electrodes with different material that may enhance its electrochemical performance [44]. Considering the unique and advantageous properties of GO, many efforts have been made towards the modification and development of these materials either by themselves, or in conjunction with other nanomaterials such as metal nanoparticles [45,46].

Among different synthetic method of nano composite structures, the ultrasonic technique has been applied in many homogeneous and heterogeneous reactions as an agitator or homogenizer. Application of ultrasound in chemical reactions provides specific activation based on an acoustic cavitation phenomenon [47]. Sonochemical preparation method utilizes the acoustic cavitation phenomenon which includes the formation of the bubbles and their successive growth and implosive collapse in a mixture of the reactant ions and clusters [48]. As a mostly adiabatic process, this collapse of the grown bubbles leads to a massive energy build-up ensuing high pressures of about 2000

atm and very high temperatures more than 5273 K (5000 °C) in localized microscopic regions inside the sonicated solution mixture [46]. It has been employed extensively for the synthesis of the nanostructured materials due to its rapid reaction rate, controllable reaction conditions, simplicity and safety. Moreover, powder particles synthesized through this method normally have uniform shape with narrow size distribution [47-49]. Response surface methodology (RSM) is an empirical mathematical model that correlates the real and simulated behavior of the adsorption efficiency to various effective parameters based on their individual and interaction effects. Central composite design (CCD) under RSM is applied for modeling and the optimization of experiments [50].

This work reports an organic functionalized graphene oxide modified using silver nanoparticles both the electrically conductivity property of graphene, hydrophilicity of choline chloride, large specific surface area and active sites to immobilize of silver nanoparticles (Ag NPs). Fig. S1 shows the covalent functionalization of graphene sheets with ChCl. One of the most significant reasons for the selection of ChCl is the presence of hydroxyl group that facilitates the attachment of it onto the surface of graphene oxide sheets through covalent bond. Moreover, the cholinium cationic polar head group ($–N^{+}(CH_3)_3$) of ChCl can provide a positively charged uniform surface with a suitable density, which can facilitate the deposition of Ag-NPs through the electrostatic interaction between $N^{+}(CH_3)_3$ and AgCl. Herein, we used of the advantages of all of the above mentioned materials and methods. We report a novel biosensor employing silver nanoparticles modified choline chloride functionalized graphene oxide (AgNPs-ChCl-GO) that was synthesized sonochemically and applied for the sensitive determination of celecoxib.

## 2. Experimental

### 2.1. Materials

Celecoxib (purity of 98%), pure graphite powder, AgCl, (2-hydroxyethyl)trimethylammonium chloride (purity of 98%), sodium hydroxide (NaOH) and $SOCl_2$ were purchased from Sigma-Aldrich company. Nitric acid, sulfuric acid and anhydrous methanol used in this investigation were of analytical grade Merck quality and used as received. Britton-Robinson buffer (B-R buffer) $4.0 \times 10^{-2}$ M was prepared by mixing $H_3PO_4$, acetic acid and boric acid with the appropriate amount of 0.2 M NaOH to obtain the desired pH. Paraffin oil from Merck was used as the pasting liquid for the preparation of the paste electrodes. A stock anhydrous ethanol solution of celecoxib ($1.0 \times 10^{-3}$ M) was prepared and kept in the dark under refrigeration (below 4 ºC). The human plasma samples were supplied from Fars Blood Transfusion Center (Shiraz, Fars, I.R. Iran).

### 2.2. Instruments

Ultrasonic Homogenizer (UHP-400) (made in Ultrasonic Technology Development company-Iran) was used for synthesis of nano particles Voltammetric measurements were carried out on Autolab PGSTAT 101 Potentiostat/Galvanostat (Metrohm Autolab, Utrecht, The Netherlands) in a conventional three electrodes glass cell (volume 250 mL, Autolab, Metrohm Autolab, Utrecht, The Netherlands) with a triple electrode configuration at ambient temperature of 25±1ºC and controlled by Nova 1.6 software. The counter and reference electrodes were platinum (Metrohm) and Ag/AgCl (Metrohm) electrodes, respectively. Differential pulse voltammetric measurements are performed at a step potential of 5 mV, pulse height of 25 mV and pulse width of 50 ms. FT-IR spectra (400–4000 $cm^{-}$ region) were recorded on the 8300-FT-IR Shimadzu spectrophotometer using KBr disks. Absorbance spectra of the solutions were recorded on a Perkin Elmer Lambda 40 UV-Vis spectrometer. A◦ X-ray powder diffraction (XRD) diffractometer (Holland Philips PW-1840) using a with monochromated Cu-Kα radiation (λ=1.54 Å), at a scanning speed of 2°/min from 20° to 80°($2\theta$) was used for elucidation of Nanostructures and estimation of crystalline size by Debye-Scherrer formula. Scanning electron microscopy (SEM) measurements were carried out using a Philips XL30 scanning electron. Fluorescence measurements were carried out on a Varian Cary Eclipse fluorescence spectrophotometer. pH in the range 1–13 was measured on pH/Ion meter model 686 (Metrohm, Switzerland Swiss).

## 2.3 Synthesis

### 2.3.1 Synthesis of AgNPs-ChCl-GO

The preparation of silver nanoparticles modified choline chloride functionalized graphene oxide in some consecutive stages that are shown in Scheme 1. The graphite oxide (GO) was prepared by a modified Hummers method [51]. For acylation of GO, 1.0 g of it was dispersed in DMF (20 mL) under ultrasonic treatment for 1 h and the process followed in the presence of $SOCl_2$ (60 mL) at 80 °C for 30 min [52]. In order to the preparation of Choline chloride functionalized graphenoxide, ChCl (0.4 g) in 8 mL THF was mixed to the $SOCl_2$ treated GO under sonochemical condition for 2 h, followed by the addition of $N(Et)_3$ (5 mL). Then, this mixture was stirred for 24 h, resulting in a stable suspension. The obtained solid was then centrifuged, separated and washed with distilled water and absolute ethanol several times. Finally, the product was dried at 60 °C overnight. In the next step, the ultrasound-assisted preparation of silver nanoparticles was performed in two continuous steps: Firstly, the AgCl has been adsorbed onto the choline chloride functionalized graphene oxide via positively charged ammonium groups by immersing 0.5 g of functionalized graphene oxide in 50.0 mL of $0.1\times10^{-3}$ M aqueous AgCl solution at room temperature. The synthesized solid has been centrifuged and washed three times with distilled water. Then, the functionalized graphene oxide has been sonicated in aqueous solution of $NaBH_4$ (50.0 mL and $1.0\times10^{-2}$ M) for 30 min. The final solid was then centrifuged, washed with distilled water and dried at 300 K.

<Scheme 1>

### 2.3.2. Preparation of AgNPs -ChCl -GO modified CPE

To prepare of carbon paste electrode (CPE), graphite powder (0.45 g) was mixed to the 0.3 mL of paraffin oil and then was packed into the hole of the electrode body and smoothed on a filter paper. AgNPs -ChCl -GO modified electrode, was prepared by mixing different amount of nanocomposite with 0.45g graphite. Each AgNPs -ChCl -GO paste was mixed well with an adequate amount of paraffin oil for 60 min until a homogeneous paste was obtained. The synthesis process was followed by packing and compacting of these pasted into the hole of the electrode body.

## 2.4. Design of experiments

Response surface methodology (RSM) composed of three steps such as conduction of statistical design of experiment, estimation of variables coefficient in empirical formula and final prediction of the response and investigation of model validating and adequacy [53] Central composite design (CCD) combination with response surface methodology was used to study the parameters contribution on the celecoxib preconcentration and subsequent determination in the sample. The boundary levels for each parameter were as follows:. pH of B-R buffer (1-8), amount of modifier (5-25 mg) and scan rate (10-50 $mVs^{-1}$) (Table 1) was taken as response. The CCD model [54] which is the standard RSM, was employed on the basis STATISTICA software (version 10.0) for the survey of effective parameters in the performance of biosensor.

Experimental data were fitted to a second-order polynomial equation, and regression coefficients were obtained.

Comparisons of means were performed by one-way ANOVA (analysis of variance), followed by t-test ($p$-value < 0.05) [55]. By calculating Adj. $R^2$ and square. $R^2$ the suitability of the response surface model was judged. The t-value indicates whether the means of two parameters are statistically different from each other or not. The larger the t-value, the smaller the p-value, and therefore, the more significant the parameter [56].

< Table 1.>

## 3. Results and Discussion

## 3.1. Characterization of AgNPs-ChCl-GO

The FT-IR spectra were recorded to investigate the chemical structure and the possible boundary of products, as depicted in Fig. 1 for the GO (a), pure ChCl (b) and AgNPs-ChCl-GO (c), at a frequency range of 4000 to 400 $cm^{-1}$. The FT-IR spectrum of the GO revealed a strong peak at 3425 which can be attributed to the hydroxyl groups. Also, the C-H, C-OH, C-O-C, C=O, C=C, C-O stretching vibrations appeared at 2931, 1750, 1610, 1437, 1231 and 882 $cm^{-1}$ [57]. In Fig. 1 (b) the stretching vibrations at 3367, 1089 and1044 $cm^{-1}$, corresponded to OH, C-C-O respectively (Fig. 1b) [57]. In addition, there are also peaks indicating the presence of a specific group of quaternary ammonium compounds, in the range of 900-1000 $cm^{-1}$. The absorption peaks which shown at the wavelength of 972 and 935 $cm^{-1}$ are suspected to be the peaks of the C-N group of ChCl, respectively [58]. The comparison of FT-IR spectrum of AgNPs-ChCl-GO (Fig. 1c) and (Fig. 1b) no change was observed at location of C-C frequency due to the presence of $Ch^{+}$ in the nanocomposite structure [59].

< Fig. 1>

The surface morphology of the AgNPs-ChCl-GO nanocomposites was studied through AFM, FE-SEM and Energy-dispersive X-ray spectroscopy analysis. The AFM image (Fig. 2a) of the nanocomposite demonstrates a high order of the surface morphology of the prepared modified GO. It is very important that the prepared composite is homogenous because its surface morphology affects the performance of the sensor with respect to parameters such as sensitivity, repeatability and detection precision. Fig. 2b presents the representative FE-SEM image of free-standing GO nanosheets, revealing a crumpled and rippled structure which was the result of deformation upon the exfoliation and restacking processes. These nanoscaled single- or few-layer GO nanosheets were flat, which were due to the sonication in the synthetic process destroyed the van der Waals interactions between GO layers, and the existence of a large amount of oxygen-containing functional groups on the surface of GO nanosheets.

As shown in Fig. 2c. A distinct change was observed between the free-GO morphology and free-standing nanosheets of AgNPs-ChCl-GO nanocomposites. It showed a nanocomposite with the sizes from 100 nm to several micrometers. This change in morphology reveals the presence of Ch groups on GO surfaces. It can be seen that the formed silver nanoparticles are spherical shaped and homogeneously dispersed in the choline chloride functionalized GO nanocomposites.

< Fig. 2.>

The energy dispersive X-ray spectroscopy spectrum of the AgNPs-ChCl-GO nanocomposite was measured to assess its chemical composition (Fig. 2d, 2e and 2f ). It showed that the composite was composed mainly of C, O, N,

Cl, and Ag elements. The appearance of a sharp peak at 0.48 KeV can show the successful oxidation of the grahen. The corresponding EDX spectrum exhibited the characteristic peaks of elemental Cl at 2.43 and 2.65 that evidences the presence of ChCl on the surface of GO. In addition, this spectra confirmed the presence of Ag nanoparticles which were successfully decorated the surface of GO film by this method. This observation is consistent with the XRD results.

Fig. 3 shows the XRD analysis of GO (A) choline chloride functionalized GO (B) and AgNPs-ChCl-GO (C). The characteristic 2θ peak of graphene oxide appeared at 12.31° corresponds to a d-spacing of approximately 0.75 nm that is consistent with the interlayer space of graphene oxide sheets in according to Braggs law [60], due to the existence of oxygen-rich groups on both sides of the sheets and water molecules trapped between the sheets In addition, two strong peaks at 12.31° and 42.56°, are attributed to the (002) plane of GO and (100) plane of the hexagonal structure of carbon, respectively [61].

The powder XRD profile of Choline chloride shows appearance of 18 peaks with 2θ values of 16.47°, 22.21°, 28.76°, 29.11, 29.84°, 30.65°, 34.65°, 36.44°, 41.78°, 45.26°, 50.14°, 50.62°, 51.35°, 51.98°, 54.21°, 58.45°, 70.76° and 72.23°[57], while, the choline chloride functionalized GO presented of peaks at 12.3, 17.5, 21.4, 22.6, 24.3, 26.8, 27.9, 30.9, 32.7, 34.8, 43.8, 44.53, 46.5, 49.9, 53.2, and 55.2 indicating the interaction between the GO and choline chloride during the modification as observed in the FT-IR study (Fig. 3b). The obtained curve has contained a peak at 12.0 degree for GO. According to the Bragg equation, the distance between sheets of graphene oxide was 0.75 nm whereas after modification of particles this distance reached to 0.80 nm. Increasing of this distance is related to presence of choline chloride agents on the surface of graphene oxide sheets [62]. Fig. 3c shows the XRD patterns of the as-synthesized AgNPs-ChCl-GO, indicating that the metal Ag was formed after being reduced by $NaBH_4$ solution. In Fig. 3c, some Bragg reflections corresponding to the (111), (200), (220), (311) and (222) sets of lattice planes are observed. These peaks are matched with the face centered cubic (fcc) structure of silver (Fig. 3d, JCPDS file No. 04-0783) [63] as shown in Fig. 3c.

The appearance of peaks at 2θ = 21.4° and 43.8° revealed the presence of choline chloride agents on the surface of graphene oxide sheets. The suggested mechanism is that the attached silver nanoparticles prevent the restacking of these carbon sheets and therefore the characteristic diffractions peaks of the layered structure disappear [64]. These figures demonstrated that the silver nanoparticles modified choline chloride functionalized graphene oxide had been prepared successfully, in accordance with the SEM, AFM and EDX results.

< Fig. 3.>

## 3.2. Electrochemical detection of celecoxib

Fig.4 shows the electrochemical results of sensing evolution of CPE, GO/CPE, GO-ChCl/CPE, and AgNPs-ChCl-GO/CPE electrodes. The voltammetric measurements of celecoxib showed that optimal electrocatalytic efficiency was achieved using the AgNPs- ChCl-GO-based sensor. The bare carbon paste electrode shows no change towards celecoxib. In the presence of GO/CPE, the reduction peak current enhanced that can be attributed to the larger surface area of the modified electrode using graphene oxide which leads to an increased conductivity. After the addition of ChCl and AgNPs to the surface of the electrode the reduction response towards celecoxib greatly increased which was due to the high capability of electric conductivity and quick electron transfer rate in the surface of the modified electrode.

< Fig. 4.>

## 3.3. CCD modeling and RSM plots

RSM is more advantageous than the traditional single parameter optimization and leads to saving in time and raw material. There were a total of 16 runs for optimizing the four individual parameters in the current CCD and ANOVA programs. By applying multiple regression analysis on the experimental data, the response variable and the test variables were related by the following equation:

$$W= 5.76543 - 3.67654\ X - 0.56720\ X^2 + 2.58432\ Y + 1.98253\ Y^2 - 2.56772\ Z + 1.73194\ Z^2 - 0.30870\ XY + 0.46895\ XZ+2.11648\ YZ$$

Where W, X, Y and Z are the response, pH, Modifier% and scan rate respectively. In this equation, the positive values indicate their positive effect on the response and the magnitude of parameters effect can be examined.

Actuals are obtained by performing the experiments whereas predicted responses are estimated from the model as proposed by the software. The $R^2$ is calculated by the ratio between the variation explained by the model and the total variation of the experimental data. Higher value of $R^2$ is desirable as it is interpreted as the percentage of variability in the response explained by statistical model. The value of $R^2$ ($R^2$ =0.982) and adjusted $R^2$ ($R^2$ adj = 0.964) are close to 1 which are very high and indicate a high correlation between the observed and the predicted values. Therefore, the response surface model established in this study for predicting of celecoxib removal was considered reasonable. By applying the diagnostic plots provided by RSM (such as the predicted versus actual value

plots), the adequacy of the modeled approximation can be estimated. The predicted values of extraction recovery of of celecoxib obtained from the model were in good agreement with the obtained experimental data (Fig. S2A).

The normal probability of residuals (Fig. S2B) indicates almost no serious violation of the assumptions underlying the analyses. Satisfactory normal distribution of results confirm the normality assumptions made earlier and the independence of the residuals. Pareto chart (Fig. S3) was used to visualize the estimated effect of variables. The chart showed that the terms X, Y, $Y^2$ have significant effect on the peak current. Analysis of variance (ANOVA) is statistical method that partitions the total variation into its component parts while each term has different source of variation and estimated the interaction. As demonstrated in Table 2 and Fig. S4, all the previous observations have been substantiated. The no significant value of lack of fit (more than 0.05) represent validity of quadratic model for explanation of experimental data of the present study. Obviously, the linear terms of pH and modifier% have larger effect with respect to scan rate. The increasing of the modifier percentage shows positive effect on the response, whereas negative response would result upon changing pH=5 to high value and it was not seen significant change before pH=5.0 (Fig. 5).

<Table. 2>

< Fig. 5.>

## 3.4. Analytical qualifications and calibration plot

DPVs experiments were performed in the presence of AgNPs-ChCl-GO in B-R buffer pH 5.0 solutions containing various concentrations of celecoxib under optimized conditions. The resulting cyclic voltammograms (Fig. 6) indicated the electrochemical reduction of celecoxib that is presented by the cathodic peak at -1.1 V, so that the corresponding reductive reaction is in direct correlation with the increased drug concentration in the solution. According to the inset of Fig 6, it was found that the intensity of the reductive peak current vs. of celecoxib concentration showed linear calibration curve with approximately two orders of magnitude from $9.6 \times 10^{-9}$- $7.4 \times 10^{-7}$, the regression equation was I (mA)=1.543C + 0.946 ($R^2$=0.990). The limits of detection were determined according to a signal-to noise-ratio (S/N) of three and the limits of quantification as ten times the above mentioned ratio, where S is the standard deviation of the background. LOD value was found to be $2.51 \times 10^{-9}$ M, while the LOQ value was found to be $6.58 \times 10^{-9}$ M. The resultant intraday and interday precisions, were calculated 1.98% and 1.96%, respectively. The peak current of the modified electrode does not change after storage in air for two weeks and it retained 92.0% of its initial response up to one month.

< Fig. 6.>

## 3.5. Application of AgNPs-ChCl-GO sensor for human plasma sample

AgNPs-ChCl-GO electrochemical biosensor was used to evaluate celecoxib concentration in human plasma sample. In order to preparation of Human plasma sample, firstly, 0.5 mL $HClO_4$ 2.0 M was added to the 1.0 mL of the sample and then centrifuged for 10 min at 1500 rpm. Here after, the supernatant diluted five times and then used for analysis of celecoxib by standard addition method. So, the prepared sample spiked with different volumes of of celecoxib standard solution in B-R buffer solution of pH 4.0. of celecoxib was determined after the addition of 0.5 µM to the human plasma samples, diluted 7 times and the spiked values were calculated from the standard addition plot. The standard addition calibration curve was constructed for determination of of celecoxib in real sample showed a straight line in the linear dynamic range with the regression equation I(mA)= 9.337 C+0.630 ($R^2$=0.996). An average value of 0.487 µM has been obtained for of celecoxib in real samples (Fig. 7), which shows a good agreement with the value of spiked. The comparison of AgNPs-ChCl-GO with other reported works for detection of celecoxibe support the efficiency of the proposed sensor (Table 3).

< Fig. 7.>

<Table. 3>

## 4. Conclusion

In this study, ultrasound-assisted synthesized silver-NPs was loaded on the chlorin chloride functionalized graphen oxide for modification of carbon paste electrode which was applied to detection of celecoxib. Central composite design and the response surface methodology were applied to optimize of experimental parameters. Differential pulse voltammetry exhibited expanded linear dynamic ranges of $9.6 \times 10^{-9}$- $7.4 \times 10^{-7}$ M for of celecoxib with a LOD (S/N = 3) and LOQ (S/N = 10) of $2.51 \times 10^{-9}$ M and $6.58 \times 10^{-9}$ M respectively. The peak current of the modified electrode does not change after storage in air for two weeks and it retained 92.0% of its initial response up to one month. The resultant intraday and interday precisions, were calculated 1.98% and 1.96%, respectively. The brilliant advantages of AgNPs-ChCl-GO-carbon paste electrode such as cost effective, simplicity, stability, recycle ability and low detection limit make it an excellent choice to detection and determine of celecoxib in biological samples.

## References

[1]. F.M. Christensen, Pharmaceuticals in the environment—A human risk?, Regul. Toxicol. Pharmacol. 28 (1998) 212–221.

[2]. C.A. Kinney, E.T. Furlong, S.L. Werner, J.D. Cahill Presence and distribution of wastewaterderived pharmaceuticals in soil irrigated with reclaimed water Environ Toxicol Chem. 25 (2006) 317-26.

[3]. I. Ali, H. Y. Aboul-Enein, K. Kummerer, Analyses of drugs and pharmaceuticals in the environment, In Biophysico-Chemical Processes of Anthropogenic Organic Compounds in Environmental Systems, IUPAC Sponsored Book Series. pp 439-462, Wiley, USA (2011), ISBN 978-0-470-94446-2.

[4]. B. P. Imbimbo,V. Solfrizzi, F. Panza, Are NSAIDs Useful to Treat Alzheimer's Disease or Mild Cognitive Impairment? Front Aging Neurosci. 2 (2010) 19.

[5]. D Jaturapatporn, M.G. Isaac, J. McCleery, N. Tabet, Aspirin, steroidal and non-steroidal antiinflammatory drugs for the treatment of Alzheimer's disease, Cochrane Database Syst Rev. (2012) 2:CD006378. doi: 10.1002/14651858.CD006378.pub2.

[6]. G. Chawla, P. Gupta, R. Thilagavathi, A.K. Chakraborti, A.K. Bansal, Characterization of solid-state forms of celecoxib, European Journal of Pharmaceutical Sciences 20 (2003) 305–317.

[7]. M.N. Najafi, M. Ghaedi, S. Moghimi-Araghi, Water propagation in two-dimensional petroleum reservoirs, Physica A: Statistical Mechanics and its Applications, 445 (2016) 102-111.

[8]. E.A. Dil, M. Ghaedi, A.M. Ghaedi, A. Asfaram, A. Goudarzi, S. Hajati, M. Soylak, S. Agarwal, V.K. Gupta, Modeling of quaternary dyes adsorption onto ZnO–NR–AC artificial neural network: Analysis by derivative spectrophotometry, Journal of Industrial and Engineering Chemistry, 34 (2016) 186-197.

[9]. M. Ghaedi, A.M. Ghaedi, B. Mirtamizdoust, S. Agarwal, V.K. Gupta, Simple and facile sonochemical synthesis of lead oxide nanoparticles loaded activated carbon and its application for methyl orange removal from aqueous phase, Journal of Molecular Liquids, 213 (2016) 48-57.

[10]. E. Nemutlu, S. Kir, Method development and validation for the analysis of meloxicam in tablets by CZE, Journal of Pharmaceutical and Biomedical Analysis, 31 (2003) 393-400.

[11]. S.E. Vignaduzzo, P.M. Castellano, T.S. Kaufman, Method development and validation for the simultaneous determination of meloxicam and pridinol mesylate using RP-HPLC and its application in drug formulations, J Pharm Biomed Anal, 46 (2008) 219-225.

[12]. M. Ghasempourabadi, A. Arshadi, A. Ghaedi, S. Shahri, High-Performance Renovation of Iranian Historical Buildings to Substitute Active Lighting Systems with Natural Light (Case Study: Shahi Bank, Tehran), Energy Procedia, 78 (2015) 777-781.

[13]. S. Hajati, M. Ghaedi, Z. Mahmoudi, R. Sahraei, SnO2 nanoparticle-loaded activated carbon for simultaneous removal of Acid Yellow 41 and Sunset Yellow; derivative spectrophotometric, artificial neural network and optimization approach, Spectrochimica Acta Part A: Molecular and Biomolecular Spectroscopy, 150 (2015) 1002-1012.

[14]. M. Brito Martínez, N. Jullok, Z. Rodríguez Negrín, B. Van der Bruggen, P. Luis, Membrane crystallization for the recovery of a pharmaceutical compound from waste streams, Chemical Engineering Research and Design 92 (2014) 264-272.

[15]. V.S. Priya, L. Philip, Treatment of volatile organic compounds in pharmaceutical wastewater using submerged aerated biological filter, Chem. Eng. J. 266 (2015) 309-319.

[16]. F. Mahdizadeh, S.I Aber, A. Karimi, Synthesis of nano zinc oxide on granular porous scoria: Application for photocatalytic removal of pharmaceutical and textile pollutants from synthetic and real wastewaters, J Taiwan Inst Chem E 49 (2015) 212-219.

[17]. M. Magureanu, N. B. Mandache, V. I. Parvulescu, Degradation of pharmaceutical compounds in water by non-thermal plasma treatment, Water Res. 81 (2015) 124-136.

[18]. S. O. Ganiyu, E. D. van Hullebusch, M. Cretin, G. Esposito, M. A. Oturan, Coupling of membrane filtration and advanced oxidation processes for removal of pharmaceutical residues: A critical review, Sep. Purifi. Technol. 156 (2015) 891-914.

[19]. I. Ali, Z. A. AL-Othman, A. Alwarthan, Synthesis of composite iron nano adsorbent and removal of ibuprofen drug residue from water, J. Mol. Liq. 219 (2016) 858-864.

[20]. I. Ali, U. Kulsum, Z. A. ALOthman, A. A. Alwarthan, K. Saleem, Advances in analyses of profens in biological and environmental samples by liquid chromatography, Curr. Pharm. Anal., 12 (2016) 158-176.

[21]. L. Moulahcene, M. Skiba, O. Senhadji, N. Milon, M. Benamor, M. Lahiani-Skiba, Inclusion and removal of pharmaceutical residues from aqueous solution using water-insoluble cyclodextrin polymers, Chem. Eng. Res. Des. 97 (2015) 145-158.

[22]. F. Wang, B. Yang, H. Wang, Q. Song, F. Tan, Y. Cao, Removal of ciprofloxacin from aqueous solution by a magnetic chitosan grafted graphene oxide composite, J. Mol. Liq. 222 (2016) 188-194.

[23]. G. Z. Kyzas, J. Fu, N. K. Lazaridis, D. N. Bikiaris, K. A. Mati, New approaches on the removal of pharmaceuticals from wastewaters with adsorbent materials, J. Mol. Liq. 209 (2015) 87-93.

[24]. L. Chen, H.T. Lian, X.Y. Sun, B. Liu, Sensitive detection of L-5-hydroxytryptophan based on molecularly imprinted polymers with graphene amplification, Anal. Biochem. 526 (2017) 58-65.

[25] R. Zare-Dorabei, S. Moazen Ferdowsi, A. Barzin, A. Tadjarodi, Highly efficient simultaneous ultrasonic-assisted adsorption of Pb(II), Cd(II), Ni(II) and Cu (II) ions from aqueous solutions by graphene oxide modified with 2,20-dipyridylamine: Central composite design optimization, Ultrasonics Sonochemistry 32 (2016) 265–276

[26] R. Zare-Dorabei, V.Jalalat, A. Tadjarodi, Central composite design optimization of Ce(III) ion removal from aqueous solution using modified SBA-15 mesoporous silica, New J. Chem., 00 (2015) 1-3.

[27] R. Zare-Dorabei, M. Shamsedini Darbandsari, A. Moghimi, M. Saghanejhad Tehrani, S. Nazerdeylami, Synthesis, characterization and application of Cyclam-modified magnetic SBA-15 as a novel sorbent and its optimization by central composite design for adsorption and determination of trace amount of lead ions, RSC Adv., 6 (2016)108477-108487.

[28] M. Saghanejhad Tehrani, R. Zare-Dorabei, Competitive removal of hazardous dyes from aqueous solution by MIL-68(Al): Derivative spectrophotometric method and response surface methodology approach, Spectrochimica Acta Part A: Molecular and Biomolecular Spectroscopy, 160 (2016) 8-18.

[29] Kh. Dashtian, R. Zare-Dorabei, Synthesis and characterization of functionalized mesoprous SBA-15 decorated with Fe3O4 nanoparticles for removal of Ce (III) ions from aqueous solution: ICP–OES detection and central composite design optimization, Journal of Colloid and Interface Science, 494 (2017) 114-123.

[30] M. Saghanejhad Tehrani, R. Zare-Dorabe, Highly efficient simultaneous ultrasonic-assisted adsorption of Methylene Blue and Rhodamine B onto Metal Organic Framework MIL-68(Al): Central composite design optimization, RSC Adv., 6 (2016) 27416-27425.

[31] S. Nourozi, R. Zare-Dorabei, Highly efficient ultrasonic-assisted removal of methylene blue from aqueous media by magnetic mesoporous silica: experimental design methodology, kinetic and equilibrium studies, Desalination and Water Treatment, 85 (2017) 184–196.

[32] R. Zare-Dorabei, R. Rahimi, A. Koohi, S. Zargari, Preparation and characterization of a novel tetrakis(4-hydroxyphenyl)porphyrin - graphene oxide nanocomposite and application in an optical sensor and determination of mercury ion. RSC Adv., 5 (2015) 93310-93317

[33]. M. Kumar, J.X. Piao, S.B. Jin, J.H. Lee, S. Tajima, M. Hori, Low temperature plasma processing for cell growth inspired carbon thin films fabrication. Archives of Biochemistry and Biophysics, 605 (2016) 41–48.

[34]. C. Lee, X. Wei, J.W. Kysar, J. Hone, Measurement of the elastic properties and intrinsic strength of monolayer graphene. Science, 321 (2008) 385–388.

[35]. A.A. Balandin, S. Ghosh, W. Bao, I. Calizo, D. Teweldebrhan, F. Miao, Superior thermal conductivity of single-layer graphene. Nano Lett, 2 (2008) 902–7.

[36]. K.I. Bolotin, K.J. Sikes, Z. Jiang, M. Klima, G. Fudenberg, J. Hone, Ultrahigh electron mobility in suspended graphene. Solid State Commun. 46 (2008):351–5.

[37]. O. Parlak, A.P.F. Turner, A. Tiwari On/Off-switchable zipper-like bioelectronics on a graphene interface. Adv Mater .26 (2014) 482–486

[38]. M.D. Stoller, S. Park, Y. Zhu, J. An, R.S. Ruoff, Graphene-based ultracapacitors. Nano Lett, 8 (2008) 3498–502.

[39]. M. Govindhan, M. Amiri, A. Chen, Au nanoparticle/graphene nanocomposite as a platform for the sensitive detection of NADH in human urine. Biosens. Bioelectron. 66 (2015) 474–480.

[40]. W. Wang, D. He, J. Duan, S. Wang, H. Peng, H. Wu, M. Fu, Y. Wang, X. Zhang, Simple synthesis method of reduced graphene oxide/gold nanoparticle and its application in surface-enhanced raman scattering. Chem. Phys. Lett. 582 (2013) 119–122.

[41]. D. Sharma, S. Kanchi, M.I. Sabela, K. Bisetty, Insight into the biosensing of graphene oxide: Present and future prospects, Arabian Journal of Chemistry, 9 (2016) 238-261.

[42]. J. I. Paredes, S. Villar-Rodil, A. Martı´nez-Alonso, J.M.D. Tasco´n, Graphene Oxide Dispersions in Organic Solvents, Langmuir, 24 (2008) 10560-10564.

[43]. M. Roosta, M. Ghaedi, A. Daneshfar, R. Sahraei, Ultrasound assisted microextraction-nano material solid phase dispersion for extraction and determination of thymol and carvacrol in pharmaceutical samples: Experimental design methodology, Journal of Chromatography B, 975 (2015) 34-39.

[44]. C. Zhu, G. Yang, H. Li, D. Du, Y. Lin, Electrochemical sensors and biosensors based on nanomaterials and nanostructures, Anal Chem, 87 (2015) 230-249.

[45]. M.F. Hossain, J.Y. Park, Palladium nanoparticles on electrochemically reduced chemically modified graphene oxide for non-enzymatic bimolecular sensing. RSC Advances 3 (2013) 16109–16115.

[46]. H.K. Jeong, Y.P. Lee, M.H. Jin, E.S. Kim, J.J. Bae, Y.H. Lee, Thermal stability of graphite oxide. Chem Phys Let. 470 (2009)255–258.

[47] H. Kalhori, A. Irajizad, A. Azarian, R. Ashiri, Synthesis and characterization of electrochemically grown CdSe nanowires with enhanced photoconductivity, Journal of Materials Science Materials in Electronics 26 (2014) 1395–1402.

[48] A. Moghtada, R. Ashiri, Superiority of sonochemical processing method for the synthesis of barium titanate nanocrystals in contrast to the mechanochemical approach, Ultrasonics Sonochemistry, 41 (2018) 127-133.

[49] A. Moghtada, R. Ashiri, Nanocrystals of $XTiO_3$ (X = Ba, Sr, Ni, $Ba_xTi_{1-x}$) materials obtained through a rapid one-step methodology at 50 C, Ultrasonics Sonochemistry, 26 (2015) 293-304.

[50]. M.A. Mohamed, A.M. Yehia, C.E. Banks, N.K. Allam, Novel MWCNTs/graphene oxide/pyrogallol composite with enhanced sensitivity for biosensing applications, Biosens Bioelectron, 89 (2017) 1034- 1041.

[51]. M. Ghaedi, A. Daneshfar, A. Ahmadi, M.S. Momeni, Artificial neural network-genetic algorithm based optimization for the adsorption of phenol red (PR) onto gold and titanium dioxide nanoparticles loaded on activated carbon, Journal of Industrial and Engineering Chemistry, 21 (2015) 587-598.

[52]. E. Roy, S. Patra, D. Kumar, R. Madhuri, P.K. Sharma, Multifunctional magnetic reduced graphene oxide dendrites: synthesis, characterization and their applications, Biosens Bioelectron, 68 (2015) 726-735.

[53]. R. H. Myers, D. C. Montgomery and C. M. Anderson-Cook, Response surface methodology: process and product optimization using designed experiments, John Wiley & Sons, 2009.

[54]. P. Salehi, F. M. Tajabadi, H. Younesi and Y. Dashti, Optimization of lead and nickel biosorption by Cystoseira trinodis (brown algae) using response surface methodology, CLEAN–Soil, Air, Water, 42 (2014) 243-250.

[55]. S. Bahrani, M. Ghaedi, M.J. Mansoorkhani, A. Asfaram, A.A. Bazrafshan, M.K. Purkait, Ultrasonic assisted dispersive solid-phase microextraction of Eriochrome Cyanine R from water sample on ultrasonically synthesized lead (II) dioxide nanoparticles loaded on activated carbon: Experimental design methodology, Ultrason Sonochem, 34 (2017) 317-324.

[56]. M.H. Omidi, F.N. Azad, M. Ghaedi, A. Asfaram, M.H.A. Azqhandi, L. Tayebi, Synthesis and characterization of Au-NPs supported on carbon nanotubes: Application for the ultrasound assisted removal of radioactive UO2 2+ ions following complexation with Arsenazo III: Spectrophotometric detection, optimization, isotherm and kinetic study, J Colloid Interface Sci, 504 (2017) 68-77.

[57]. R. Ashiri, Detailed FT-IR spectroscopy characterization and thermal analysis of synthesis of barium titanate nanoscale particles through a newly developed process, Vibrational Spectroscopy, 66 (2013) 24– 29.

[58]. L. Vieira, R. Schennach, B. Gollas, In situ PM-IRRAS of a glassy carbon electrode/deep eutectic solvent interface, Phys Chem Chem Phys, 17 (2015) 12870-12880.

[59]. M.N. Najafi, M. Ghaedi, Geometrical clusters of Darcy's reservoir model and Ising universality class, Physica A: Statistical Mechanics and its Applications, 427 (2015) 82-91.

[60].1 M. Hayyan, A. Abo-Hamad, M.A. AlSaadi, M.A. Hashim, Functionalization of graphene using deep eutectic solvents, Nanoscale Res Lett, 10 (2015) 1004.

[61]. L. Alidokht, S. Oustan, A. Khataee, M.R. Neyshabouri, A. Reyhanitabar, Enhanced removal of chromate by graphene-based sulfate and chloride green rust nanocomposites, Journal of the Taiwan Institute of Chemical Engineers, 68 (2016) 266-274.

[62]. A. Kaveh, A. ArefAzar, Surface Modification of Graphene Oxide and Investigation of Its Effects on Surface Properties of Aramid Membranes, Polymer-Plastics Technology and Engineering, 54 (2015) 1606-1614.

[63]. P. Kar, S. Sardar, B. Liu, M. Sreemany, P. Lemmens, S. Ghosh, S.K. Pal, Facile synthesis of reduced graphene oxide-gold nanohybrid for potential use in industrial waste-water treatment, Sci Technol Adv Mater, 17 (2016) 375-386.

[64]. M. Ghaedi, A. Shahamiri, B. Mirtamizdoust, S. Hajati, F. Taghizadeh, A novel polyvinyl chloridemembrane optical sensor for the determination of $Cu^{2+}$ ion based on synthesized (N′1E,N′2E)-N′1,N′2- bis(pyridine-2-ylmethylene)oxalohydrazide: Experimental design and optimization, Spectrochimica Acta Part A: Molecular and Biomolecular Spectroscopy, 138 (2015) 878-884.

[65]. K. Manian Manesha, P. Santhosha, Sh. Komathi a, N. H. Kima, J. W. Park, A. I. Gopalana, K. P. Lee, Electrochemical detection of celecoxib at a polyaniline grafted multiwall carbon nanotubes modified electrode, Analytica chimica acta 626(2008)1-9.

[66]. E. Arkan, Z. Karimi, M. Shamsipur, R. Saber, Electrochemical determination of celecoxib on a graphene based carbon ionic liquid electrode modified with gold nanoparticles and its application to pharmaceutical analysis. Anal Sci. 29 (2013) 855-60.

[67]. A. Nezhadali, S. Sadeghzadeh, Experimental design-artificial neural network-genetic algorithm optimization and computer-assisted design of celecoxib molecularly imprinted polymer/carbon nanotube sensor, Journal of Electroanalytical Chemistry, 795 (2017) 32-40

[68]. S. Chandran, P. R. Jaghav, P. B. Kharwade, D R. N. Saha, Rapid and Sensitive Spectrofluorimetric Method for the Estimation of Celecoxib and Flurbiprofen, Indian Journal of Pharmaceutical Sciences, 68 (2006) 20-25.

# Silver-choline chloride modified graphene oxide: novel nano-bioelectrochemical sensor for Celecoxib detection and CCD-RSM model

Zohreh Parsaee [a,*], Nima Karachi [b], Seyyed Milad Abrishamifar [c], Mohammad Reza Rezaei Kahkha [d], Razieh Razavi [e]

[a] Young Researchers and Elite Club, Bushehr Branch, Islamic Azad University, Bushehr, Iran.

[b] Department of Chemistry, Islamic Azad University, Marvdasht Branch, Marvdasht, Iran.

[c] Department of Chemical Engineering, New York international university of technology and management, New York, USA.

[d] Department of Environmental Health Engineering, Zabol University of Medical Sciences, Zabol, Iran

[e] Department of Chemistry, Faculty of Science, University of Jiroft, Jiroft, Iran.

Email address: zohreh_parsaee@yahoo.com

# Caption of Figures and Schematics

**Scheme 1.** Synthesis procedure of silver-NPs modified choline chloride functionalized graphene oxide (AgNPs-ChCl-GO)

**Fig. 1**. FTIR spectra of GO (A), choline chloride (B), and AgNPs- ChCl -GO (C).

**Fig. 2.** (**a**) The AFM image of AgNPs-ChCl-GO, (**b**) The SEM image of GO (**c**) AgNPs-ChCl-GO, (**d**) The EDX spectrum of AgNPs-ChCl-GO.

**Fig. 3.** XRD pattern of (A) GO (B) choline chloride functionalized GO (C) and AgNPs-ChCl-GO (d) XRD pattern of silver( JCPDS file No. 04-0783), (e) XRD pattern of silver( JCPDS file No. 04-0783),

**Fig. 4.** Differential voltammogrames CPE, GO/CPE, ChCl/GO/CPE and AgNPs/ChCl/GO/PG modified electrodes in presence of of 1.0 mM CEL in B–R buffer (pH 5.0).

**Fig. 5.** Response surface plot of (A) pH versus %modifier (mg) (µL) (XY), (B) scan rate (mV/s) versus pH (XZ), and (C) scan rate (mV/s) versus % modifier on current response of biosensor.

**Fig. 6.** (A) DPVs of CEL in B–R buffer solution (pH 5.0) with different concentrations of CEL at a scan rate of 50 mV $s^{-1}$. (B) Insets: the plot of the peak current as a function of CEL in the concentration range $9.6 \times 10^{-9}$- $7.4 \times 10^{-7}$.

**Fig. 7.** DPVs curves of AgNPs/ChCl/GO/CPE electrode in B-R buffer solution pH 5.0, Insets show the standard-addition calibration plot extracted from data of plot.

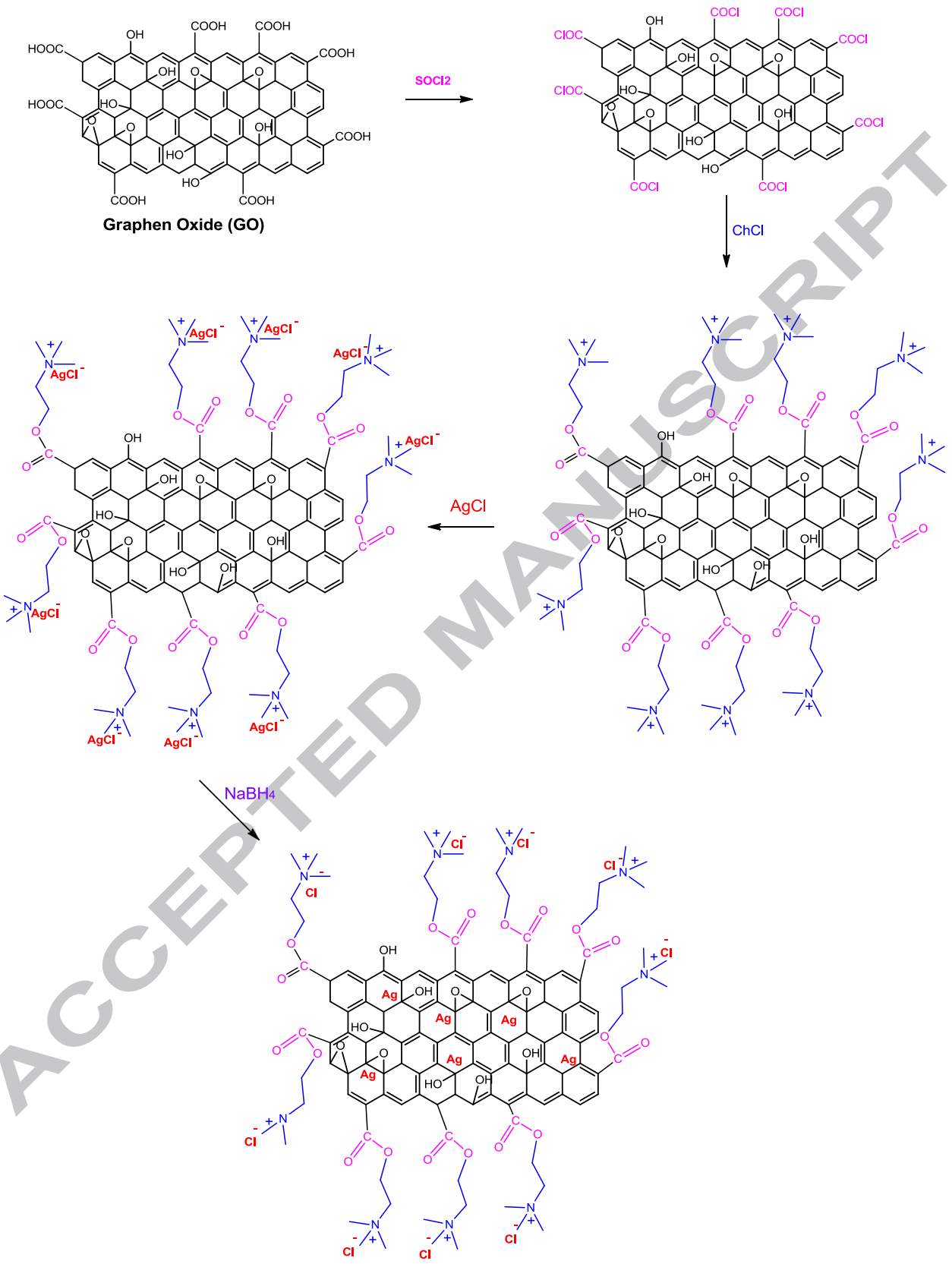

Scheme 1

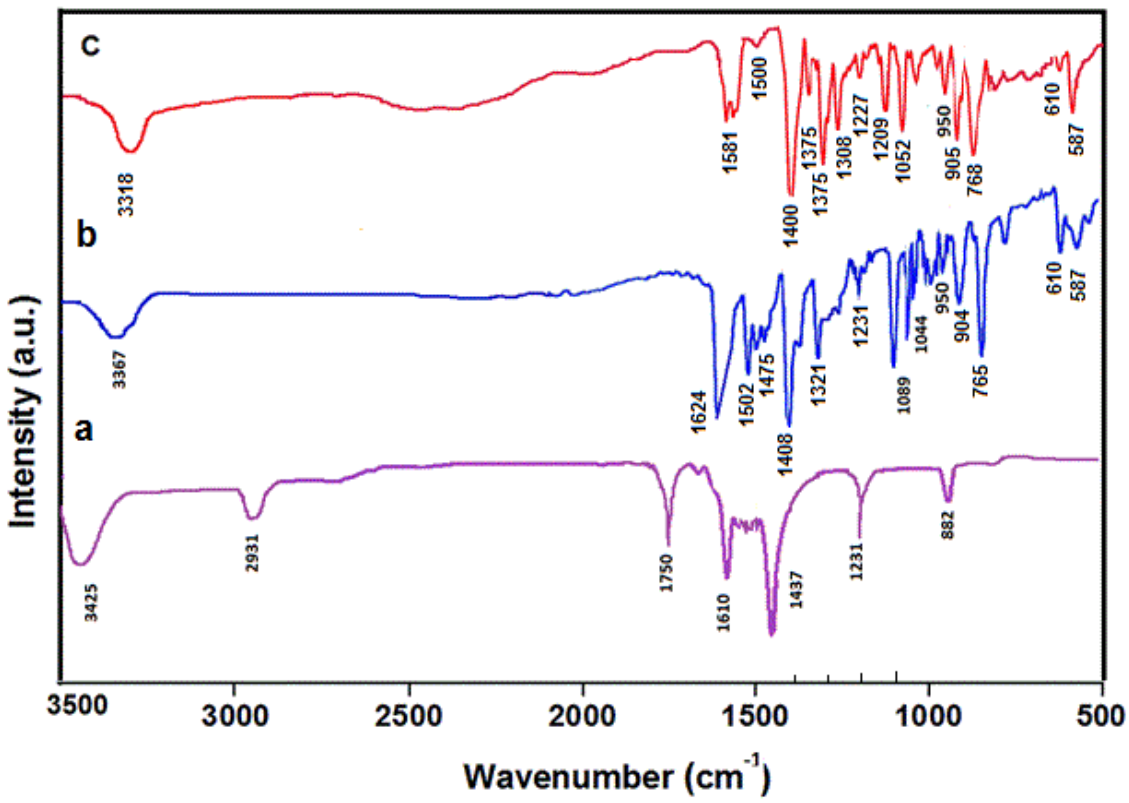


Fig. 1

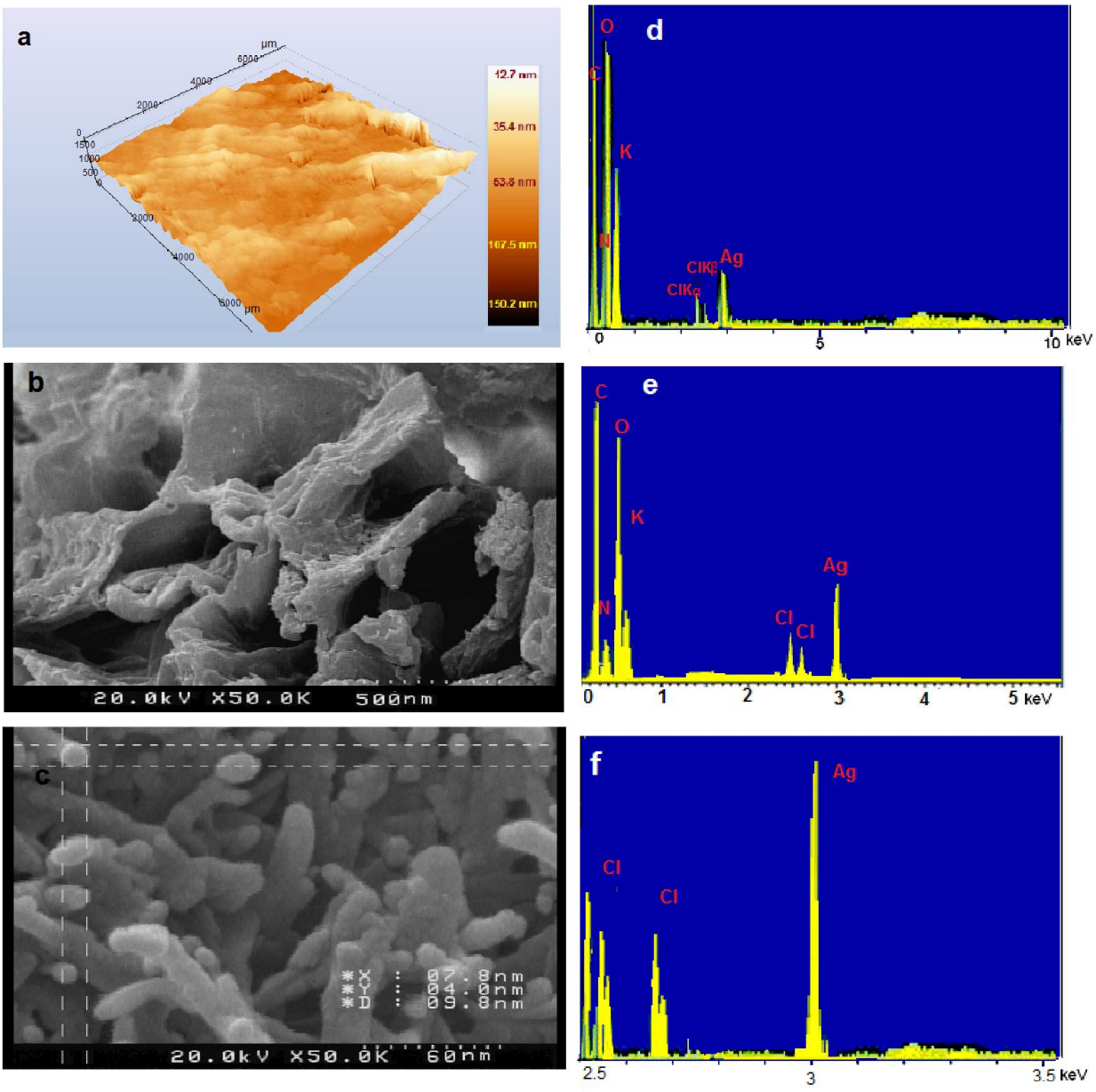


**Fig. 2**

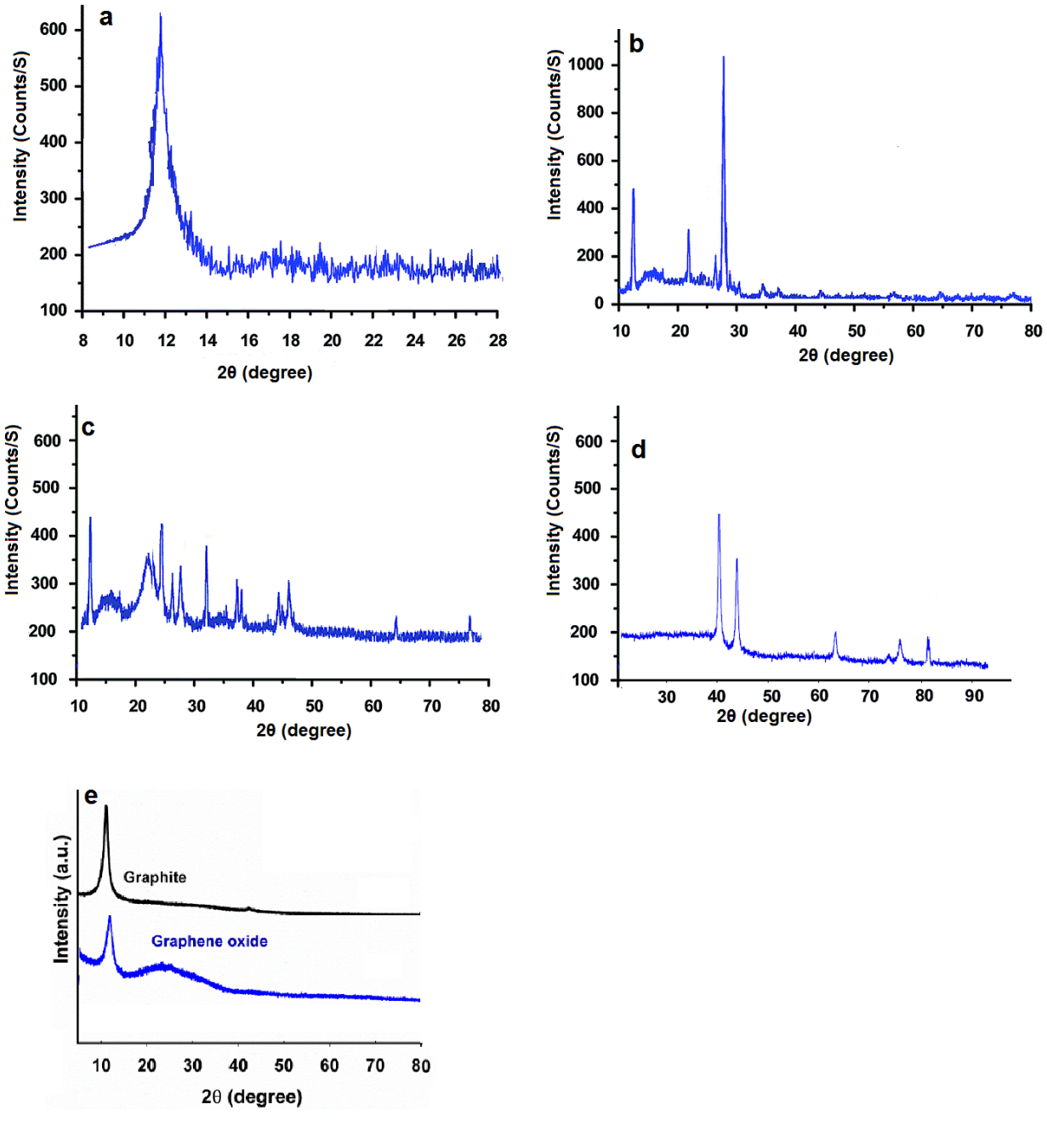


Fig. 3

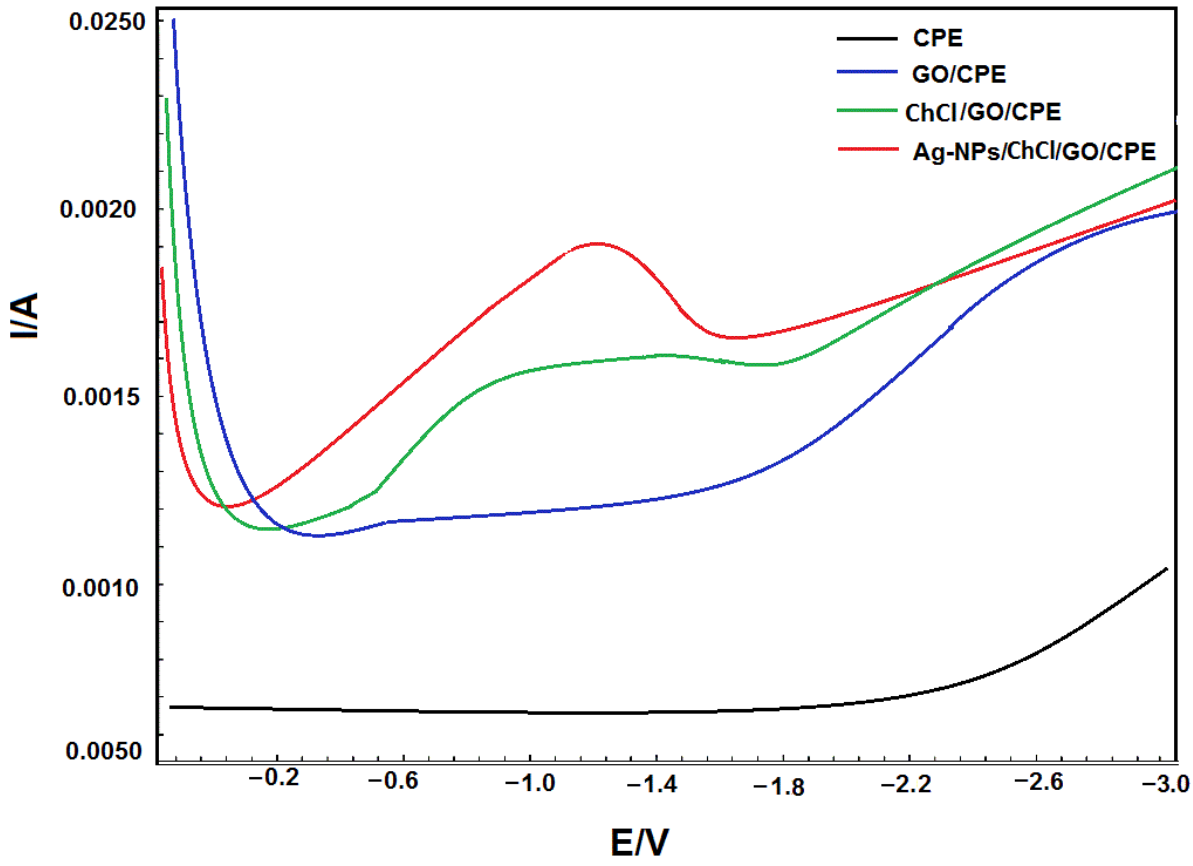


Fig. 4

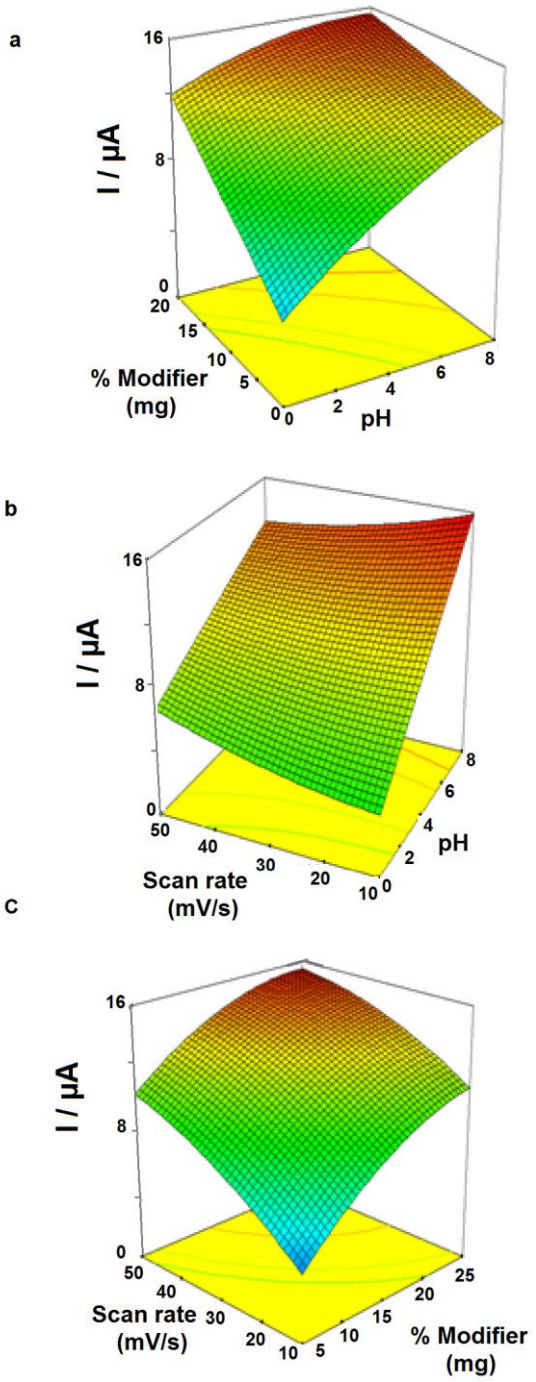


Fig. 5

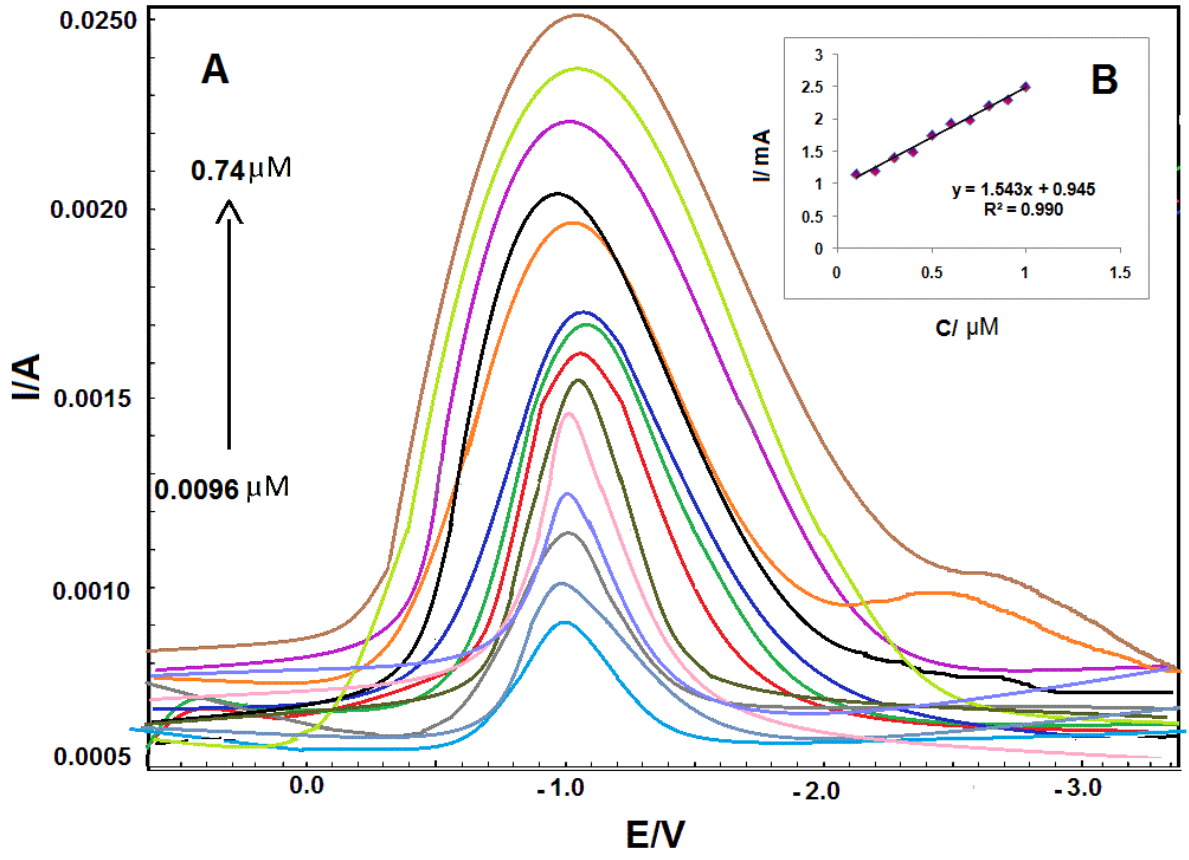


Fig. 6

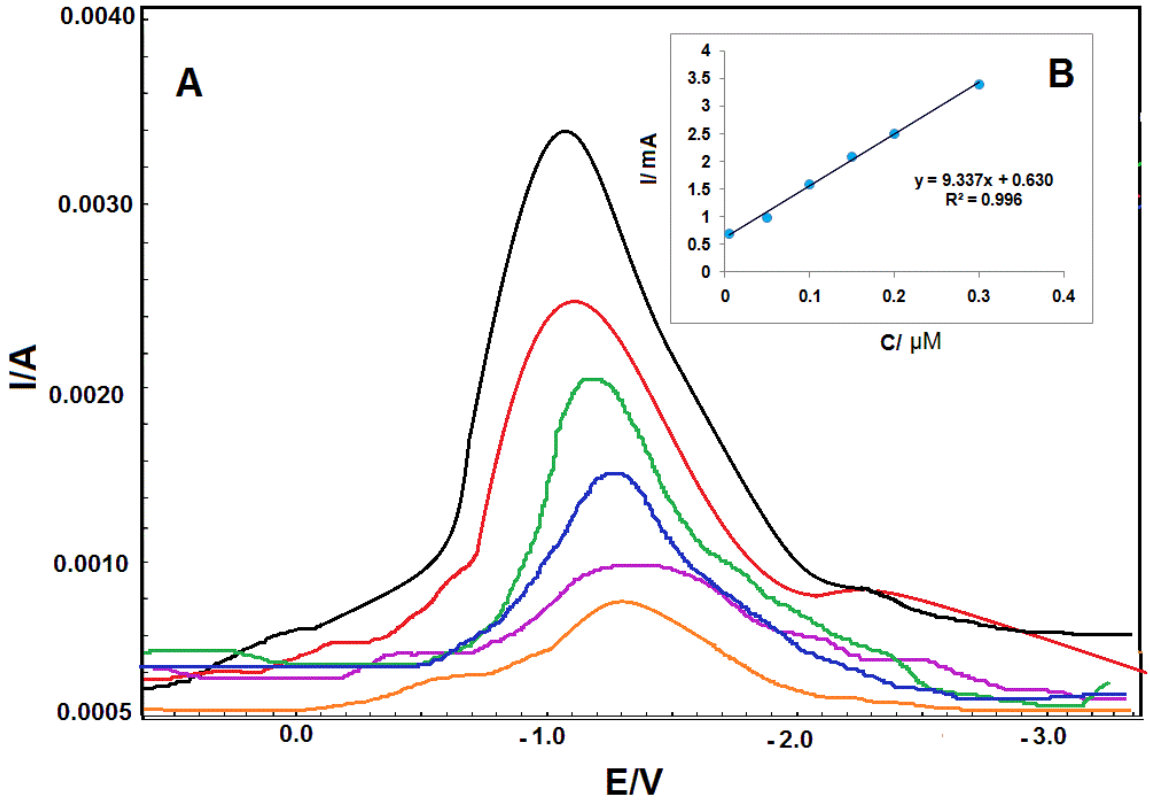


Fig. 7

# Silver-choline chloride modified graphene oxide: novel nano-bioelectrochemical sensor for Celecoxib detection and CCD-RSM model

Zohreh Parsaee [a,*], Nima Karachi [b] Seyyed Milad Abrishamifar [c], Mohammad Reza Rezaei Kahkha [d], Razieh Razavi [e]

[a] Young Researchers and Elite Club, Bushehr Branch, Islamic Azad University, Bushehr, Iran.

[b] Department of Chemistry, Islamic Azad University, Marvdasht Branch, Marvdasht, Iran.

[c] Department of Chemical Engineering, New York international university of technology and management, New York, USA.

[d] Department of Environmental Health Engineering, Zabol University of Medical Sciences, Zabol, Iran

[e] Department of Chemistry, Faculty of Science, University of Jiroft, Jiroft, Iran.

Email address: zohreh_parsaee@yahoo.com

## Caption of Tables

**Table 1.** Experimental Parameters in central composite design.

**Table 2.** Results of Analysis of variance (ANOVA) for CCD.

**Table 3.** The comparison of AgNPs-ChCl-GO with some reported works for celecoxibe detection.

**Table 1.**

| **Factors** | **levels** | | | **Star point α=2.2** | |
|---|---|---|---|---|---|
| | low | central | high | -α | +α |
| PH B-R buffer | 3.0 | 5.0 | 7.0 | 1.0 | 8.0 |
| Modifier% (mg) | 8.0 | 16.0 | 20.0 | 5.0 | 25.0 |
| Scan rate (mV/s) | 20.0 | 30.0 | 45.0 | 10.0 | 50.0 |
| **Run** | **pH B-R buffer** | **modifier% (mg)** | **scan rate (mV/s)** | **I/μA** | |
| 1 | 3.0 | 8.0 | 15.0 | 10.21 | |
| 2 | 3.0 | 8.0 | 45.0 | 8.53 | |
| 3 | 3.0 | 24.0 | 15.0 | 9.97 | |
| 4 | 3.0 | 24.0 | 45.0 | 11.14 | |
| 5 | 7.0 | 8.0 | 15.0 | 6.65 | |
| 6 | 7.0 | 8.0 | 45.0 | 5.31 | |
| 7 | 7.0 | 24.0 | 15.0 | 7.02 | |
| 8 | 7.0 | 24.0 | 45.0 | 6.84 | |
| 9 | 5.0 | 16.0 | 30.0 | 7.51 | |
| 10 | 1.0 | 16.0 | 30.0 | 10.22 | |
| 11 | 8.0 | 16.0 | 30.0 | 4.23 | |
| 12 | 5.0 | 5.0 | 30.0 | 8.34 | |
| 13 | 5.0 | 30.0 | 30.0 | 11.13 | |
| 14 | 5.0 | 16.0 | 7.5 | 9.00 | |
| 15 | 5.0 | 16.0 | 35 | 7.68 | |
| 16 | 5.0 | 16.0 | 30.0 | 7.41 | |

**Table 2.**

| Source | Sum of Squares | df | Mean Square |
|---|---|---|---|
| (1) Ph B-R solution | 38.88254 | 1 | 38.88254 |
| pH B-R solution(Q) | 0.15748 | 1 | 0.15748 |
| (2) Modifier (mg) % | 8.55241 | 1 | 8.55241 |
| %modifier (mg)(Q) | 9.01275 | 1 | 9.01275 |
| (3)scan rate (mV/s)(L) | 2.54278 | 1 | 2.54278 |
| scan rate (mV/s)(Q) | 3.59874 | 1 | 3.59874 |
| 1L by 2L | 0.24570 | 1 | 0.24570 |
| 1L by 3L | 0.52417 | 1 | 0.52417 |
| Lack of Fit | 2.54612 | 5 | 2.54612 |
| Pure Error | 0.05474 | 1 | 0.010948 |
| Total SS | 78.25411 | 17 | 78.25411 |

**Table 3.**

| Raw | sensor | Method | LOD | Ref. |
|---|---|---|---|---|
| 1 | MWNT/PANI-ME and PANI-ME | CV | $1x10^{-5}$ µM | 65 |
| 2 | graphene-based carbon ionic liquid electrode modified with gold nanoparticles | DPV | 0.2 µM | 66 |
| 3 | MIP | CV and DPV | $2.34 \times 10^{-3}$ µM | 67 |
| 4 | - | Spectrofluorimetric | 4.97 ng/ml | 68 |
| 5 | AgNPs-ChCl-GO | DPV | $2.51 \times 10^{-3}$ µM | Present work |

**Highlights**

- Modification of CPE by ultrasound-assisted synthesized Ag-NPs-Ch-GO.
- Application of a cost effective method using modified carbon paste electrode (CPE) for celecoxibe detection in biological samples.
- High selective biosensor has detected celecoxibe with LOD of $2.51 \times 10^{-9}$ M in human plasma.


1. $SOCl_2$
2. ChCl
3. AgCl

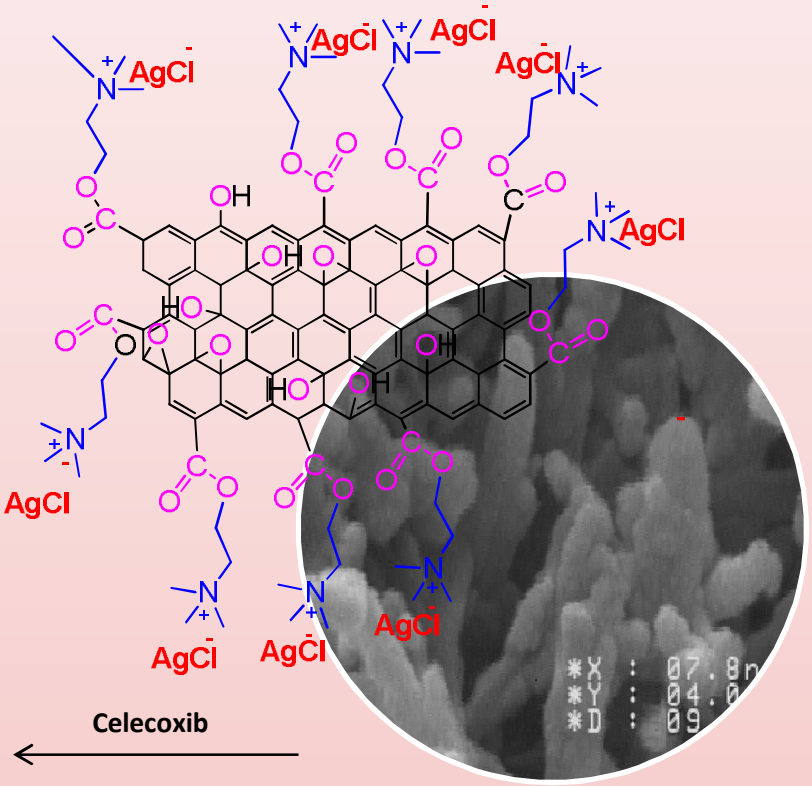


Celecoxib